ICAS 2016
30th Congress of the International Council of the Aeronautical Sciences
DCC, Daejeon, Korea ; September 25-30, 2016

STUDY OF THE UNSTEADY STRUCTURES EVOLUTION IN SHOCK WAVE / BOUNDARY LAYER INTERACTION FOR VARIOUS UPSTREAM CONDITIONS

P.A. Polivanov, A.A. Sidorenko & A.A. Maslov
Khristianovich Institute of Theoretical and Applied Mechanics SB RAS
630090, Institutskaya, 4/1, Novosibirsk, Russia
polivanov@itam.nsc.ru

Keywords: *SWBLI, transition, flow control, plasma*

Abstract

The paper deals with a parametric experimental and numerical study of the upstream boundary layer effect on stationary and non-stationary characteristics of the shock wave / boundary layer interactions (SWBLI) and the wake. Incident shock wave generated by a wedge induced the separation of the boundary layer developed on the flat plate at M=1.47. The boundary layer state was varied from laminar to turbulent by changing position of the interaction relative to the leading edge. The measurements were performed by PIV. It was found that the growth of the momentum thickness and development of coherent structures in SWBLI zone and the wake strongly depend on the state of the incoming boundary layer. The experimental data provide the database for verification of turbulence models for transitional RANS computations. The flow control plasma devices damping growth of the momentum thickness were studied experimentally.

1 Introduction

Modern trends in transonic aviation are connected with reducing of viscous drag. Therefore commercial airplanes of the next generations may be equipped with a laminar wing [1,2]. Generic feature of the transonic flow near the airfoil is presence of local supersonic zone ended by a shock wave. Laminar boundary layer has weak resistance to adverse pressure gradients especially ones produced by shock waves, in contrast to the turbulent boundary layer [3]. This leads to significant flow separation that can eliminate all advantages of laminar flow. Therefore it is necessary to estimate changes of steady and unsteady parameters of the separation zone depending on the positions of the laminar-turbulent transition relative to the zone of shock wave boundary layer interaction (SWBLI) for moderate Mach numbers. Flow separation on airfoil not only reduces the lifting force and increases drag, but also leads to additional adverse events, including buffeting [3]. It is known that separation of laminar flow usually has a greater length as compared to turbulent [4]. It was obtained [5] that for small supersonic Mach number losses of the total pressure and lifting force in SWBLI with laminar upstream boundary layer may be not worse than for turbulent conditions and this effect is more evident for high unit Reynolds numbers. The reason is fast turbulization of the shear layer in SWBLI for laminar case and significant reduction of the separation length. However in this case the big structures originated in SWBLI were found developing downstream and increasing the momentum thickness in the wake. As a result the boundary layer thickness for laminar case may be higher than for turbulent one manifesting the higher losses in the wake.
The purpose of the paper is to study development of these structures in SWBLI and an attempt to decrease their intensity with plasma devices. In addition comparison of the experimental data with the RANS calculations allow qualitatively defined as a real non-

equilibrium processes influence on transition flow at positive pressure gradient.

2 Experimental and numerical setup

The experiments were performed in wind tunnel T-325 (ITAM SB RAS) for Mach number M_∞ = 1.47, total temperature 291 K and four values of total pressure P_0 = 0.55, 0.7, 0.85 and $1.0 \cdot 10^5$ Pa (Re_1 = 8.5-15.5·10^6 m^{-1}). Test chamber of the wind tunnel has a rectangular cross section of 160x200 mm. The configuration of the experimental model is presented in Figure 1. Experimental model consisted of a plate with sharp leading edge occupying full span of the test section and a wedge generating a shock wave. In this series of experiments, the wedge angle was 3-4º. This corresponds to regular reflection of a shock wave from a wall for the inviscid case. The blockage ratio of the test section was relatively high therefore the flow start was provided by extended cavities above the wedge and below the plate. Variation of local boundary layer parameters and its state (laminar/turbulent) was provided by shifting of the flat plate in streamwise direction relatively to the wedge. To provide the same conditions near the leading edge the extension plates were installed downstream of the lower nozzle wall. Several extension plates of different length L were used. The figure shows that the distance from the flat plate leading edge to the center of the optical window is connected with length of the extension plate and is approximately equal to (380-L) mm. Position of the wedge was chosen to provide intersection of the shock wave with the model approximately in the center of the optical window. The effect of natural laminar-turbulent transition on stationary and non-stationary parameters of the SWBLI was studied for three cases L = 100, 200 and 250 mm (Approximate distance from the leading edge to the intersection the incident shock wave with the model was equal to 285, 185 and 135 mm respectively).

The main measurement techniques were PIV, Schlieren visualization and measurements of wall pressure by unsteady pressure sensors arranged along the model. Seeding of DEHS microparticles with an average size of 1 micron were used for PIV measurement.

It was found that the beginning of the transition changes from 150 to 120 mm with increasing of Reynolds number and the end of the transition changes from 210 to 180 mm. These data indicate that using of extension plate of length L = 250 mm provided laminar inflow boundary layer for all Reynolds numbers. For the case of L = 200 mm the inflow boundary layer was transitional and for L = 100 mm the boundary layer was turbulent.

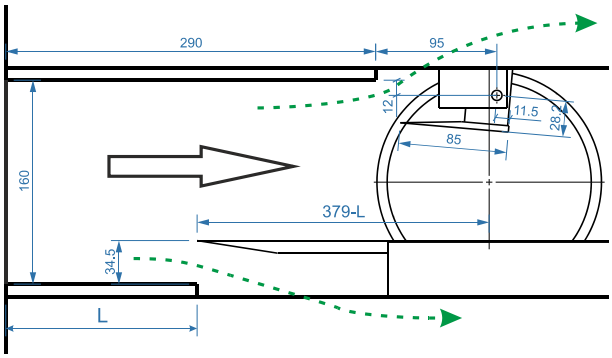

Fig. 1. The draft experimental model

The plasma control devices were studied in the experiments. The spark discharge (SD) was chosen to achieve high concentrations of the energy in the plasma region. The model with installed SD actuator in shown in Figure 2. It has ceramic insert made from MACOR holding a line of flush mounted electrodes. The electrodes are placed at distance 93 mm from the leading edge. There are three pairs of the electrodes with discharge gap of 4.5 mm. Distance between the neighbor electrode pairs is 14.5 mm. All tree discharge gaps are connected in-series. The capacitors connecting the interim electrodes to the ground were used to assist the breakdown (Figure 3).

Spark discharge actuator was fed by high voltage source using two transformers DAEHAN 15000V/30mA. From the beginning the output of the source had to be controlled by semiconductor switch MANTIGORA. Unfortunately the electronic noise produced by the spark did not allow to use this kind of switch for impulse formation. Therefore another self-adapting scheme was developed using a battery of capacitors C1 connected in parallel to the actuator (Figure 3). This capacity is charged up

to discharge level and consequently discharges. This process is periodic and the period depends on the environmental conditions and total capacity. The discharge repetition process is self-regulated therefore the frequency is not perfectly stable. In the following discussion this frequency is deduced as f=1/T where T is averaged period of the discharges.

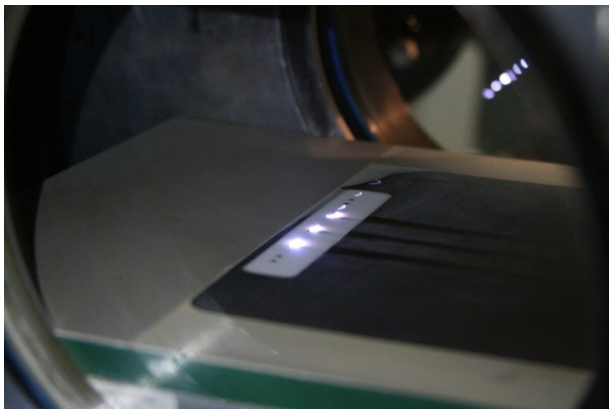

Fig. 2. Model with spark discharge actuator

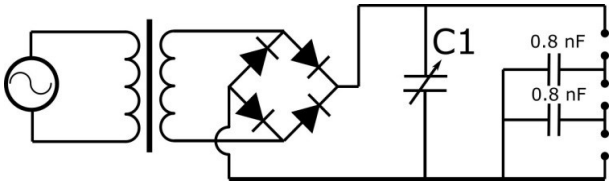

Fig. 3. Stark discharge high voltage generator

RANS simulation was done by means of commercial software Fluent using transitional SST turbulence model (SST k-w-γ-Re_θ). The computation domain was meshed to provide $\Delta y+\approx 1$, $\Delta x+\approx 10$-30. Number of cells: ≈0.5 mil. Size of calculation area: 250x91 mm. Boundary conditions correspond to experiment.

3 Experimental and numerical results

In paper [5] the correlation between pulsation of velocity in SWBLI zone and the growth of the momentum thickness was revealed. Figure 4 shows an example of the distribution of the momentum thickness in zone of interaction for the different states of the incoming boundary layer at natural laminar-turbulent transition. X_{imp} here corresponds to the point of intersection of the incident shock wave with plate for the inviscid flow, measured from the leading edge of the plate. It is clearly seen that the most rapid growth of the momentum thickness happens for the laminar case (it is accompanied by a high level of fluctuation). For transition cases this trend was not found. Also in paper [5] it was shown that the roughness can reduce the momentum thickness in the wake for the turbulent case in comparison to the case of laminar flow. But the roughness do not provide the flow similar of transitional case.

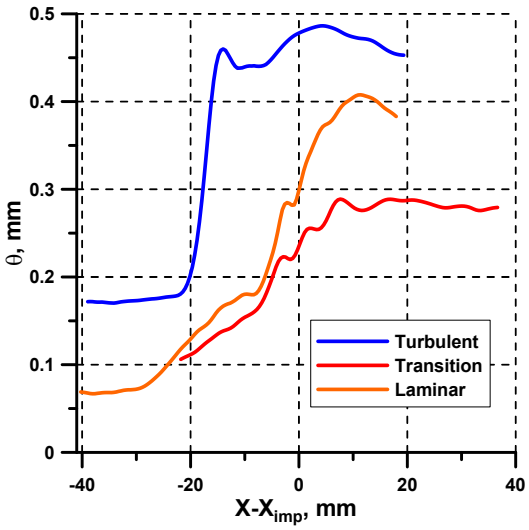

Fig. 4. The momentum thickness distribution along the SWBLI (natural conditions for $Re_1 = 13.2 \cdot 10^6$ m^{-1})

Figure 5 - Figure 7 show the combined data for turbulent, transitional and laminar test cases: distributions of mean velocity, RMS of longitudinal velocity, the correlation coefficient R_{UV} and the example of the POD analysis. It is clearly seen that for the turbulent case (Figure 5b) the pulsation of the zone of interaction leads to oscillations of the Mach stem. It was found that in the logarithmic part of the incoming equilibrium turbulent boundary layer the coefficient $R_{UV} \approx$-0.2. In the zone of SWBLI the R_{UV} significantly deviates from this value. In this zone non-equilibrium turbulent boundary layer occurs, but further downstream the correlation coefficient begins to recover. At the end of the measurement domain the coefficient $R_{UV} \approx 0.3$. Example of POD modes (Figure 5d) shows the presence of interconnected characteristic oscillations across the domain. It can be seen that some oscillations of POD mode exist in the incoming boundary layer. Perhaps the large-scale structures in the zone of SWBLI

and wake arise from the pulsations of the incoming boundary layer for turbulent case.

In the case of laminar-turbulent transition (Figure 6) high level of pulsations was found only in the shear layer. In contrast to the turbulent case where the maximum of pulsations occurs near the reflected shock wave for the transitional case the growth of pulsations is retained up to the point X_{imp}. Further downstream fullness of the velocity profile and absolute value of the coefficient R_{UV} begins to grow. It happens due to turbulization of the boundary layer. The coefficient R_{UV} near the end of the measured area is approximately equal to -0.2. This means that the turbulent boundary layer is rapidly restored to equilibrium state. For first twenty POD modes significant damping of unsteady processes was found near the end of the domain (see, for example, Figure 6d). The turbulent boundary layer arising in the zone of SWBLI for the transitional case quickly "forgets" about the interaction zone.

For the laminar case (Figure 7) the flow pattern is similar to the transition case, but there are several significant differences. First of all there is a significant growth of the pulsations and generation of thick turbulent boundary layer as a result. Absolut value of R_{UV} increases dramatically in the zone of interaction and begins to decrease downstream. A significant decrease of POD modes energy near the end of the measured zone was not found. It can be assumed that for the laminar case in the SWBLI zone strongly nonequilibrium turbulent boundary layer is generated with high level of RMS, which slowly recovers downstream. In the transitional case the process of the turbulization is more gradual.

In Figure 8 one can see the energy distribution for the first 20 modes obtained from POD analysis. The region of measurements for all cases was approximately the same, that allows to perform a quantitative comparison. The energy of structured oscillations of the flow for the laminar case significantly exceeds the values obtained for turbulent and transitional cases. Thus for laminar case the powerful coherent structures present in the interaction zone.

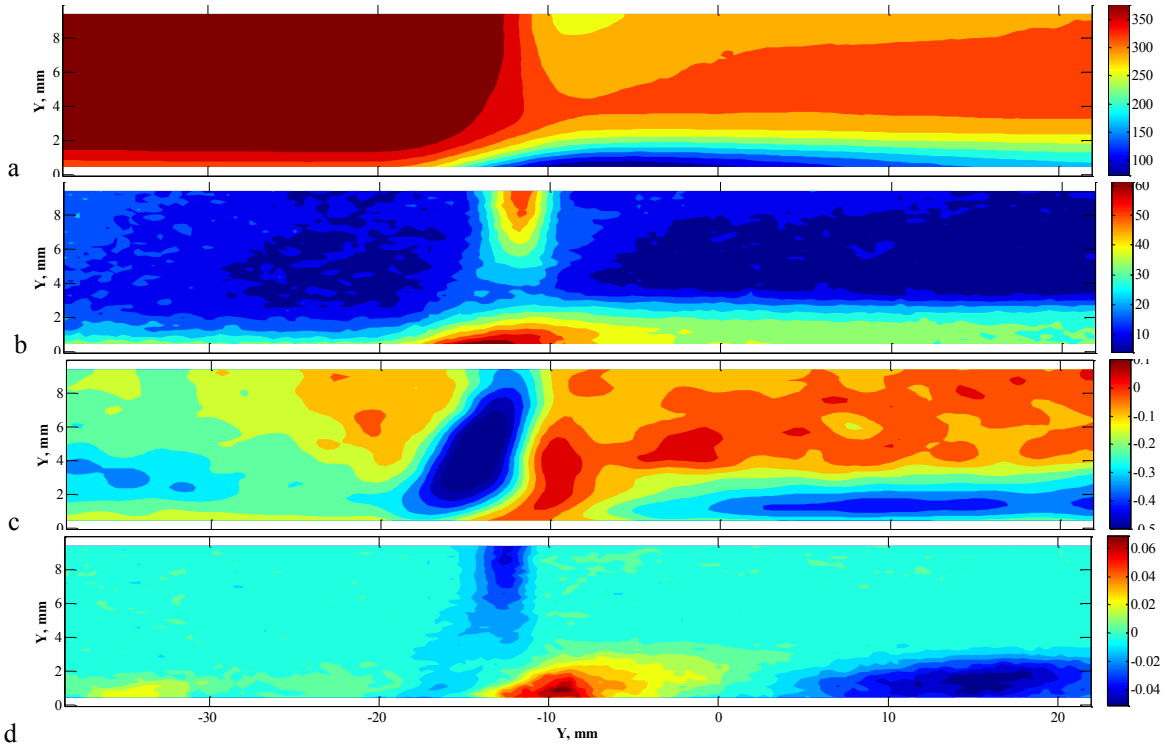

Fig. 5. a) Mean velocity, b) RMS of longitudinal velocity, c) correlation coef. R_{UV}, d) example of POD modes for turbulent inflow boundary layers ($Re_1 = 13.2 \cdot 10^6$ m^{-1}, turbulent interaction)

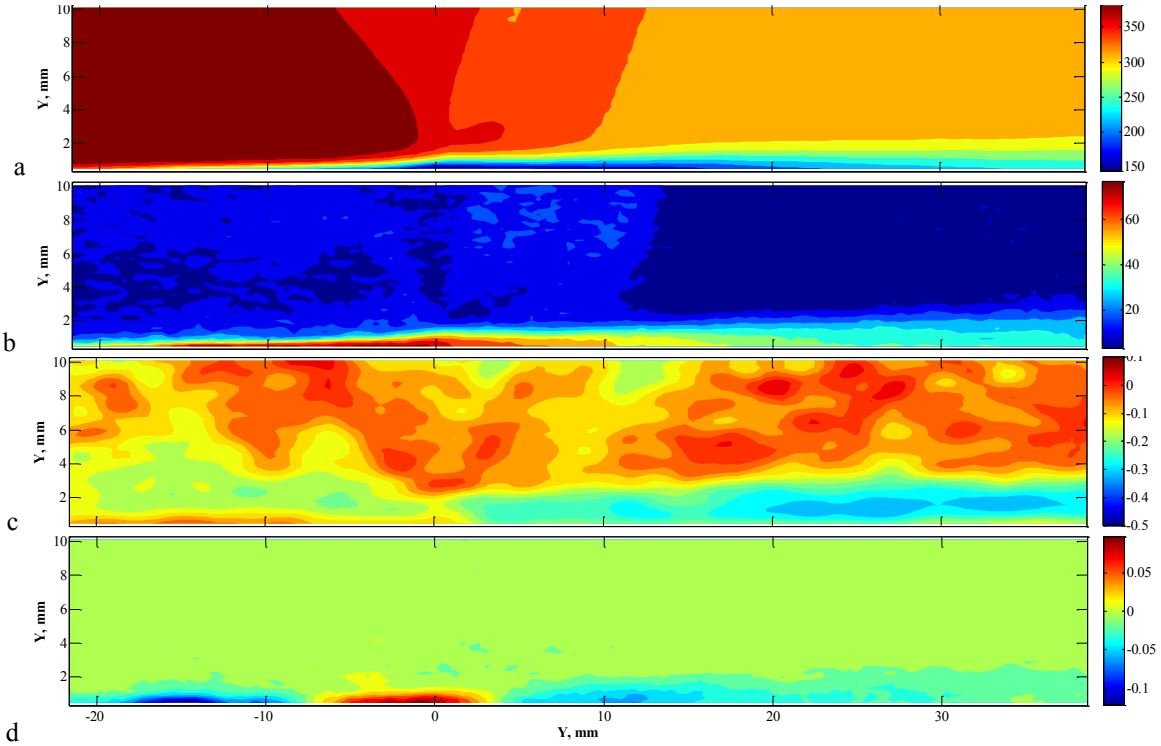

Fig. 6. a) Mean velocity, b) RMS of longitudinal velocity, c) correlation coef. R_{UV}, d) example of POD modes for transition inflow boundary layers ($Re_1 = 13.2 \cdot 10^6$ m^{-1}, transitional interaction)

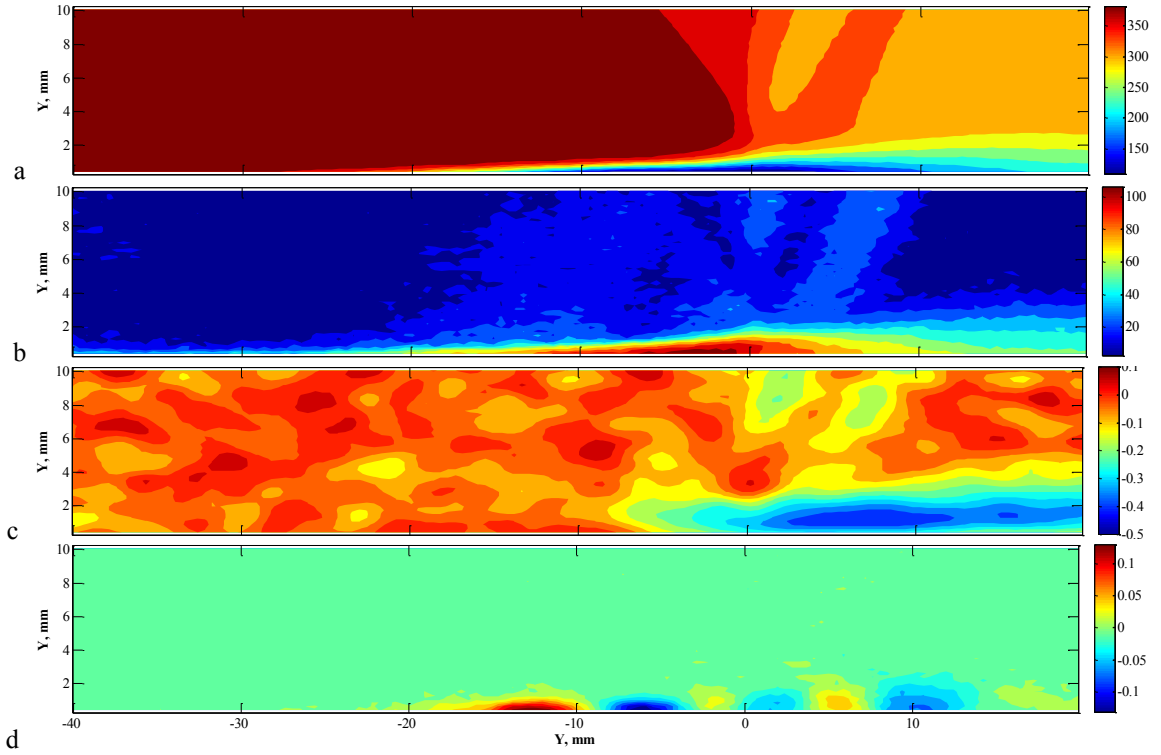

Fig. 7. a) Mean velocity, b) RMS of longitudinal velocity, c) correlation coef. R_{UV}, d) example of POD modes for laminar inflow boundary layers ($Re_1 = 13.2 \cdot 10^6$ m^{-1}, laminar interaction)

Additional measurements in the wake of the laminar case showed that boundary layer slowly become closer to the equilibrium turbulent boundary layer. But the momentum thickness in this wake varies weakly it can be assumed that the evolution of the boundary layer occurs only by redistribution of the energy accumulated in the zone of SWBLI. And the exchange of energy with the inviscid flow in the wake is weak. POD analysis shows weak damping of structures in the boundary layer in the wake.

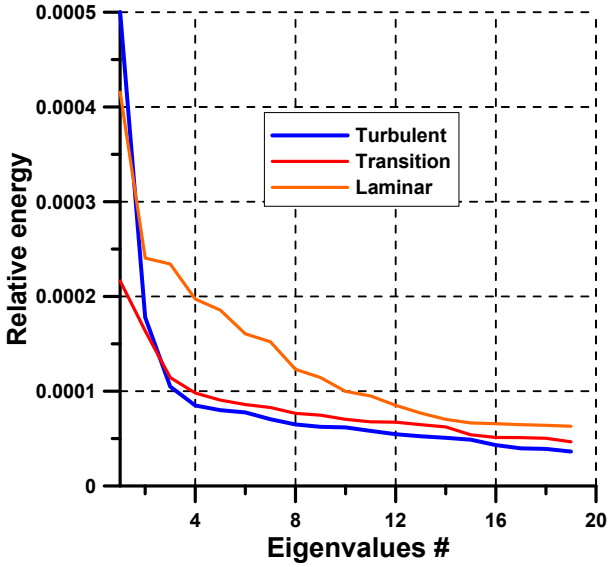

Fig. 8. Relative energy associated with mode #m

The spectrograms of pressure pulsations for turbulent case are qualitatively similar to those of most published data for the turbulent interaction (see, for example, [6,7]). More interesting data were obtained for the laminar and transitional cases.

In Figure 9-10 one can be seen the distribution of PSD*(f)·f* along the zone of interaction and the distribution of the cross-correlation between the unsteady pressure sensor located in the zone of maximum pulsations and sensor located 11 mm upstream. To reduce problems with systematic noise of amplifier the wavelet transform was applied to find cross-correlation characteristics. This technique reduced the impact of noise and allowed to obtain a distribution of cross-correlations for different frequencies.

For the transitional case in the incoming boundary layer on can see presence of a peak of pulsations with frequency of about 5-8 kHz, which may related to processes of turbulent spots origination. Correlation analysis shows that these disturbances propagate downstream. Near the point of X_{imp} there is a sharp increase of the pulsations associated with the turbulization of the boundary layer. Further downstream we can see rapid increase in the pulsations for all frequency band. This means the formation of developed turbulent boundary layer. Peak of pulsation at low frequencies (about 1 kHz) is obviously due to some feedback process (oscillation of the shock wave and separation zone). From the correlation it can be seen that disturbances up to 0.5 kHz are moving upstream in the separation region.

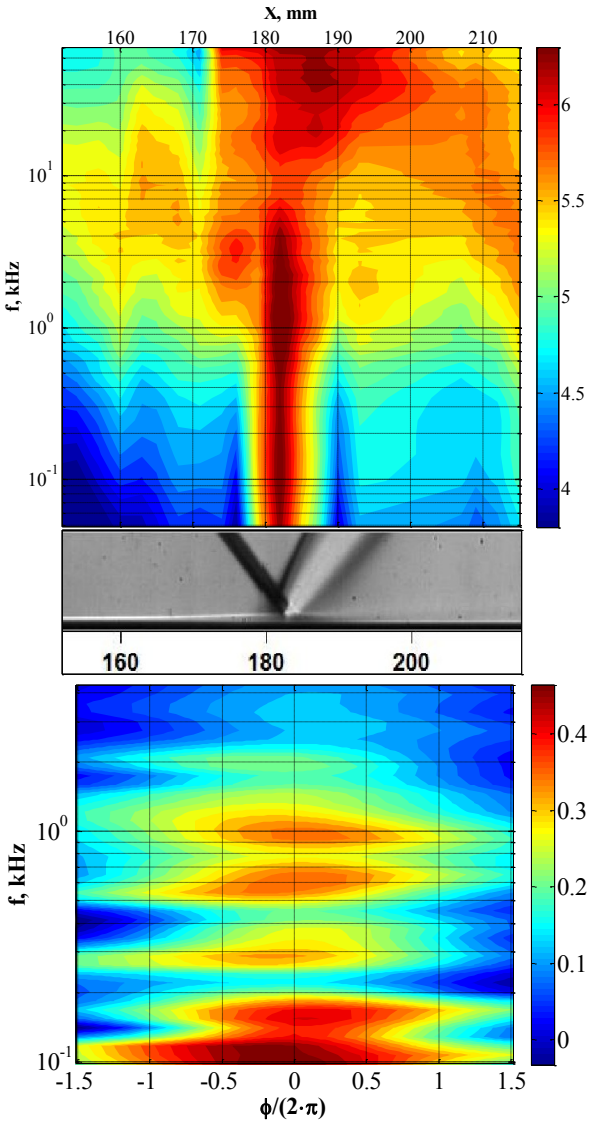

Fig. 9. Spectrogram of wall pressure pulsations and cross-correlation distribution for transition test case (L=200mm, β = 4°, P_0 = 0.7 bar)

For laminar case peak of pulsation was also found near X_{imp} and most likely associated with the beginning of the turbulization of BL. In contrast to the transitional case growth of pulsations in the wake mainly takes place only in some frequency band. This means that the boundary layer is not equilibrium. The characteristic peak of pulsations in the high-frequency range for the laminar case has a frequency of two times lower than for the transitional case (20-30 kHz against 50-60 kHz). This can be attributed by the generation of a large-scale structures for the laminar case. It is

confirmed also by POD analysis. This means that the disturbances presenting in the beginning of the laminar-turbulent transition significantly change the SWBLI and do not allow to form the large-scale structures.

In the low-frequency region two peaks of about 2 kHz and 0.2 kHz were found. These pulsations most probably are the characteristic frequencies of the separation zone and the zone of interaction. From the correlation analysis it can be seen that these disturbances (up to 2kHz) propagate upstream and originate near the point of the shock wave interaction with the boundary layer.

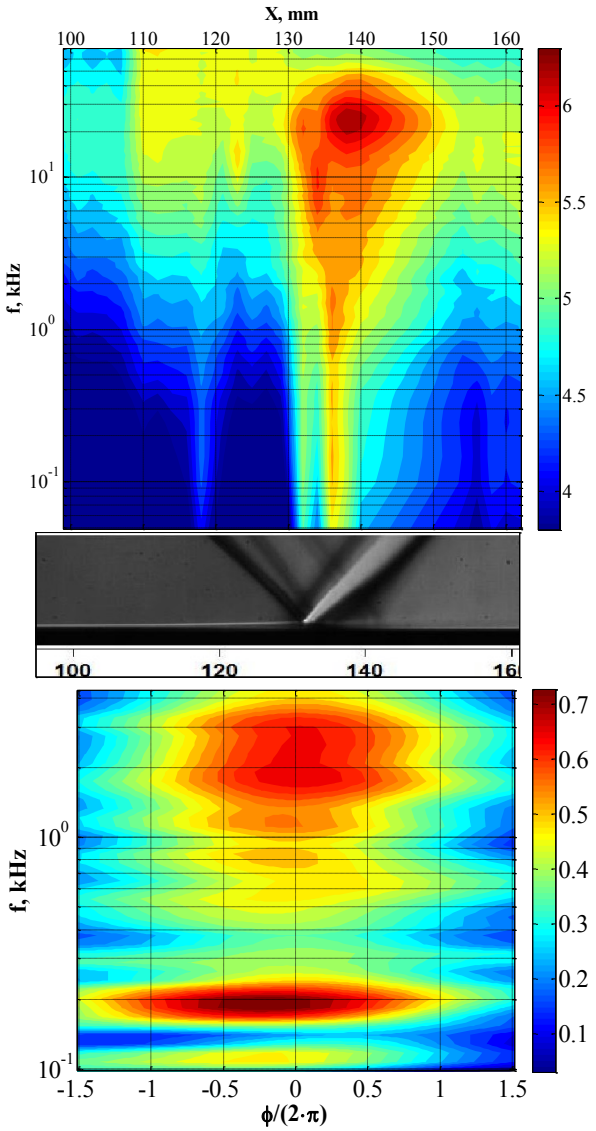

Fig. 10. Spectrogram of wall pressure pulsations and cross-correlation distribution for laminar test case (L=250 mm, β = 4°, P_0 = 0.7 bar)

These data confirms that the disturbances of the upstream boundary may greatly affect the mean flow parameters in the interaction region.

Figure 11 presents a comparison of numerical and experimental data obtained for the case of laminar upstream boundary layer. RANS simulation was done by means of commercial software. Both the experiment and CFD simulation reveal the transition and turbulization of the shear layer in the region of adverse pressure gradient. It can be seen from the figure that the length of the interaction is well predicted by CFD (for various Reynolds numbers and β) but the growth of the boundary layer is underestimated. It is most likely connected with underestimation of the fluctuation growth in RANS simulation.

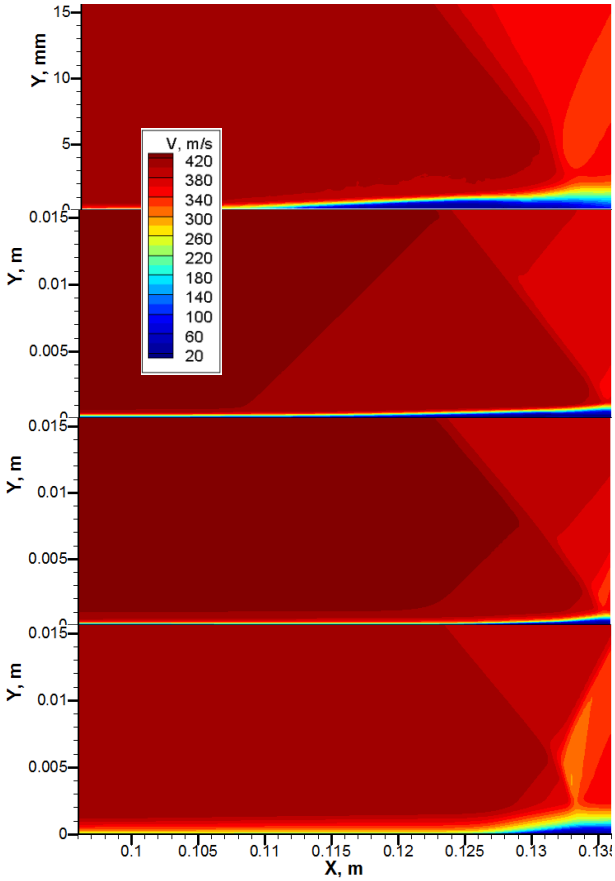

Fig. 11. Comparison of velocity profiles. Top to bottom: experiment, RANS with different level of pulsations (0.1, 1, 2 %).

Increasing the level of pulsation in calculation on the input border leads to gradual decrease the length of the interaction zone. For Tu = 2% the incoming boundary layer becomes turbulent. It was obtained that RANS calculations are

unable to provide the flow pattern matching with experimental transitional case. Therefore, this RANS model can only be used for qualitative analysis of SWBLI with laminar incoming BL.

Since some benefit was obtained for the transitional case in comparison with the laminar one it was decided to excite in the upstream boundary layer disturbances similar to obtained in the laminar-turbulent transition. Artificial turbulization by the roughness did not result in any benefit therefore the spark discharge was applied.

The experiments were done for laminar boundary layer (L=250 mm) and P_0 = 0.55 bar. PIV measurements were synchronized with plasma discharge using time delay unit. The current pulse duration in the spark was less than 1 us and average power for one discharge gap was estimated as P_{dis} = 11 Watt. Figure 12 shows pulse energy and frequency for several values of capacity C1.

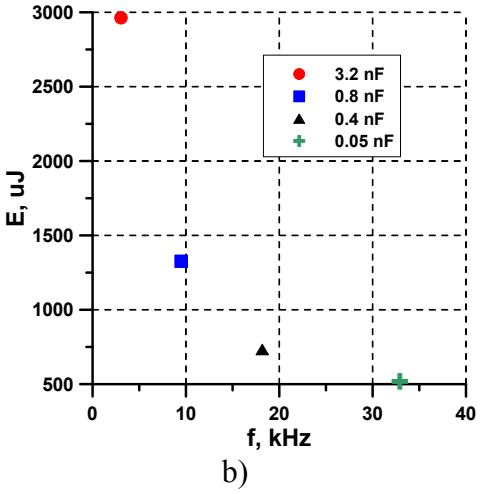

b)

Fig. 12. Discharge pulse power vs repetition frequency (average power was approximately 11 W)

The PIV data obtained for pulse energy of E_{dis} = 0.7 mJ (f = 18.2 kHz), β = 4° are shown in Figure 13. High average frequency of the discharge means that the flow disturbances produced by the sparks travel downstream with small distance between them (≈15-20 mm). Since the high voltage system is self-regulated the breakdowns are not perfectly periodical. In the experiments PIV system was triggered by a discharge and the traces of the preceding discharges present in each single velocity distribution. However in the averaged data shown in Figure 13 we can see only trace of the triggering breakdown since the delay between the sparks is not perfectly constant.

At the moment Δt=100 μs the disturbance generated by the discharge passes the interaction. It can be seen that the compression waves upstream of the interaction are concentrated close to the interaction and they are more intense in comparison with the reference laminar case. This is evidence of diminishing or disappearance of the laminar separation zone upstream of the interaction. This is similar to the turbulent test case but the reflected shock wave is weaker. Fullness of the velocity profiles increases in the interaction and downstream.

The disturbance is represented by the area of low velocity in the boundary layer due to the hot spot with low density and high temperature. Decrease of velocity in this spot is amplified when it goes through the shock wave because of changes of the shocks configuration induced by the spot.

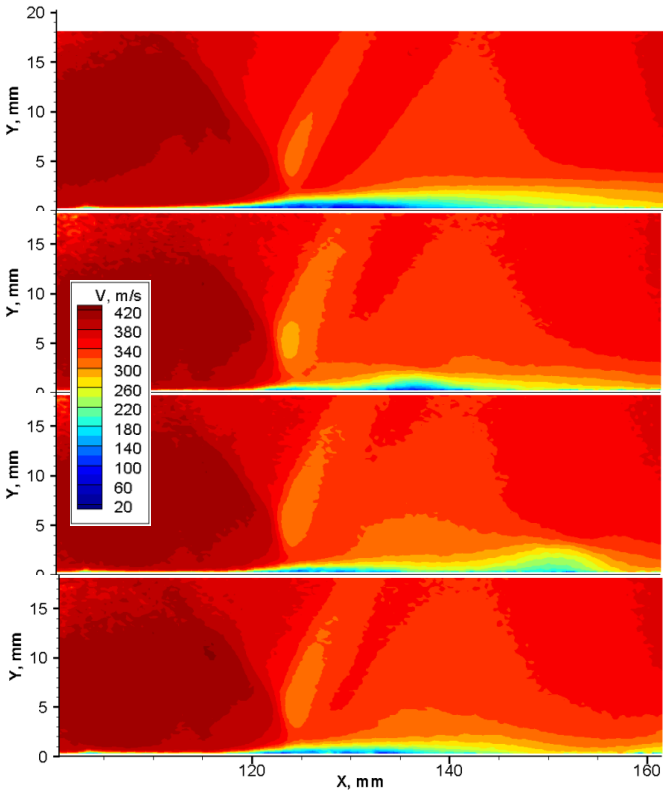

Fig. 13. Mean velocity fields at different time lag (E_{dis} = 0.7 mJ, β = 4°). Top to bottom: reference, discharge 100-220 μs with Δt = 60 μs.

RMS of velocity pulsations for this test case is presented in Figure 14. We can see high level of pulsations in the hot spot region. As the hot spot travels downstream the level of velocity pulsations decreases. It is necessary to note that level of the pulsations in the wake is generally decreased in comparison with the reference cease everywhere except the spot itself.

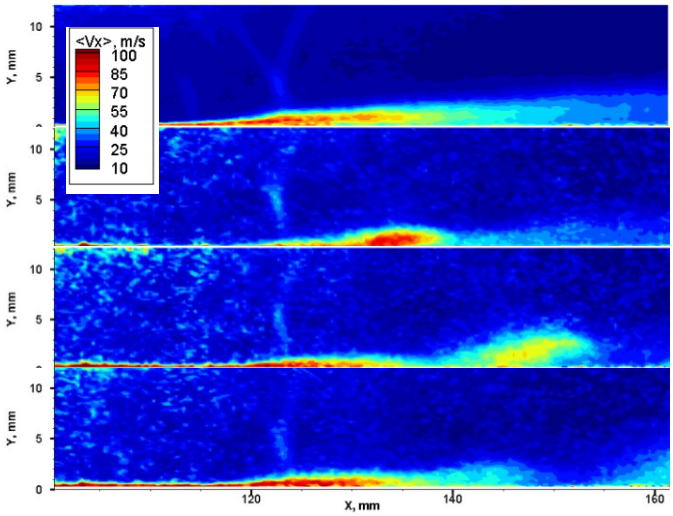

Fig. 14. RMS of longitudinal velocity at different time lag (E_{dis} = 0.7 mJ, β = 4°). Top to bottom: reference, discharge 100-220 μs with Δt = 60 μs.

Figure 15 presents the comparison of laminar and turbulent (artificial turbulization, wire trigger in position of the spar) test cases and cases with discharge excitation with various power. It can be seen that discharge actuator allows to achieve less intensive shock wave and slow growth of the wake. The best result was obtained for the lower value of spark energy.

Variation of the momentum thickness for the case of E_{dis} = 0.7 mJ, β = 4° is presented in Figure 16. It can be seen that the spark discharge is able to reduce the average momentum thickness in the wake by 30% in comparison with laminar case.

Comparison of the averaged θ distribution with instantaneous ones presented in the same figure shows that in the region of the hot spot there is increase of losses. Therefore the positive effect of the disturbances provided by the discharge may be eliminated by the hot spot.

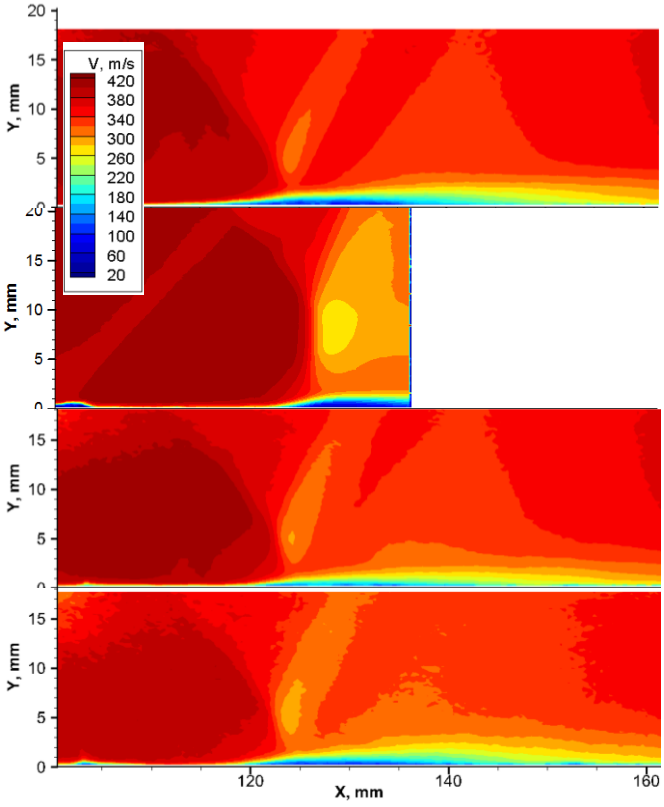

Fig. 15. Mean velocity fields at β = 4°. Top to bottom: laminar case, turbulent case, average discharge case E_{dis} = 0.7 mJ, E_{dis} = 1.3 mJ

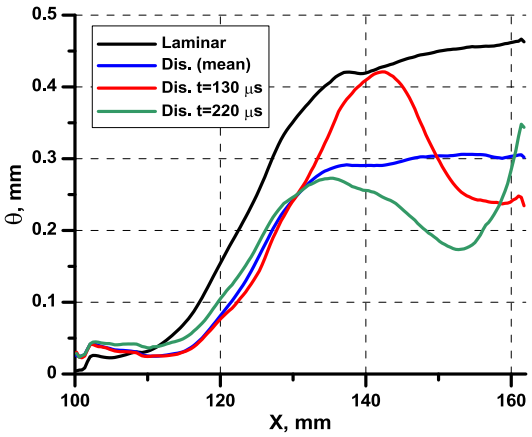

Fig. 16. Distribution of the (a) momentum thickness along SWBLI (E_{dis} = 0.7 mJ, β = 4°).

The flow control efficiency may be estimated basing on θ value at the end of measurement region as $\eta_{dis}=0.5\rho\cdot U^3(\theta_{lam}-\theta_{dis})/P_{dis}$. For β = 4° the maximum value of efficiency η_{dis}=225% was obtained for minimum spark energy E_{dis} = 0.7 mJ. If the spark energy was increased up to E_{dis} = 1.3 mJ the efficiency dropped to 167 %. Increase of spark energy up to 3 mJ resulted in negative efficiency -55%. This means that the disturbance generated by the spark is sufficient

but there in negative effect provided by the hot spot increasing with the power. This conclusion agrees with results of computational study [8] where some optimum of pulse energy was found for the flow turbulization by a discharge. In the case of exceed of energy the effect diminishes due to heat spot formation. Since the flow parameters of study [8] and the presented experiments are close it can be assumed that decrease of energy by 10 will allow to keep positive effect and increase the control efficiency.

4 Conclusions

It was found that the evolution of the turbulent boundary layer in the wake strongly depends on the state of the boundary layer upstream of SWBLI. It was found that for the laminar case the turbulent boundary layer generated in the zone of interaction quickly takes energy from the inviscid flow due to formation of large coherent structures. For the transitional case this effect was not found. As a result, the viscous losses for the transitional case are substantially less in comparison with the laminar and turbulent cases.
Spark discharge actuators were tested and found to be effective to excite powerful periodic disturbances and control the interaction region. Basing on the quantitative analysis it may be concluded that spark discharge actuator improves the average flow in the interaction region. The analysis shows that active flow control may be more effective in comparison with passive control by the roughness.

The work was supported by EU in framework of FP7 TFAST project and the Grant of President of the Russian Federation for State support of young Russian scientist – Candidates of sciences No Mk- 6682.2016.1.

References

[1] E. Allison, I. Kroo, P. Sturdza, Y. Suzuki, H. Martins-Rivas. Aircraft Conceptual Design with Natural Laminar Flow. 27th International Congress of the Aeronautical Sciences. 2010.

[2] J.E. Green. Laminar Flow Control - Back to the Future? AIAA Paper 2008-3738.

[3] B.H.K. Lee. Self-sustained shock oscillations on airfoils at transonic speeds. Progress in Aerospace Sciences. 2001. Vol. 37. pp. 147-196.

[4] M. Swoboda and W. Nitschef. Shock Boundary-Layer Interaction on Transonic Airfoils for Laminar and Turbulent Flow. Journal of aircraft. 1996. Vol. 33. No. 1. pp. 100-108.

[5] P.A. Polivanov, A.A. Sidorenko, A.A. Maslov. Transition Effect on Shock Wave / Boundary Layer Interaction at M=1.47. AIAA Paper 2015-1974.

[6] J.P. Dussage, P. Dupont and J.F. Debieve. Unsteadiness in shock wave boundary layer interaction with separation. Aerospace Science and Technology. 2006. No. 10. pp. 85-91.

[7] P.A. Polivanov, A.A. Sidorenko and A.A. Maslov, Correlation study in shock wave-turbulent boundary layer interaction, An International Journal on Shock Waves, Detonations and Explosions. 2011. Vol. 2. N. 3. pp. 193-203.

[8] P.A. Polivanov, A.A. Sidorenko, A.A. Maslov. Artificial turbulization of the supersonic boundary layer by dielectric barrier discharge. 29th Congress of the International Council of the Aeronautical Sciences. 2014.

5 Contact Author Email Address

Polivanov P.A. – polivanov@itam.nsc.ru
Sidorenko A.A. – sindr@itam.nsc.ru

Copyright Statement